SCIENCE CHINA
Earth Sciences

• RESEARCH PAPER •

May 2017 Vol.60 No.5: 943–957
doi: 10.1007/s11430-016-9029-7

Early Paleozoic granulite-facies metamorphism and anatexis in the northern West Qinling orogen: Monazite and zircon U-Pb geochronological constraints

MAO XiaoHong[1,2], ZHANG JianXin[1*], YU ShengYao[3,4], LI YunShuai[5], YU XingXing[1,2] & LU ZengLong[1]

[1] *Institute of Geology, Chinese Academy of Geological Sciences, Beijing 100037, China;*
[2] *School of Earth and Space Sciences, Peking University, Beijing 100871, China;*
[3] *Submarine Geosciences and Prospecting Techniques, MOE and College of Marine Geosciences, Ocean University of China, Qingdao 266100, China;*
[4] *Laboratory for Marine Geology, Qingdao National Laboratory for Marine Science and Technology, Qingdao 266235, China;*
[5] *Institute of Surface-Earth System Science, Tianjin University, Tianjin 300072, China*

Received September 26, 2016; accepted March 7, 2017; published online March 28, 2017

Abstract In the northern West Qinling orogen (WQO), granulite-facies metamorphic rocks are recognized within the Qinling Complex. These rocks are composed of amphibole-bearing two-pyroxene granulite and garnet-sillimanite gneiss with widespread migmatitization. We investigate three granulite-facies samples and one leucosome sample from the Qinling Complex, which are suitable for U-Pb analyses of zircon and monazite. SHRIMP and LA-ICPMS U-Pb age dating of zircon and monazite from two pelitic granulites provides weighted mean ages of 430±4 Ma (MSWD=0.88) and 433±4 Ma (MSWD=0.27), respectively. Based on the petrographic characteristics and zircon CL imagery, we postulated a ca. 430 Ma metamorphic timing for the pelitic granulites. LA-ICPMS zircon U-Pb data from an amphibole two-pyroxene granulite sample reports two weighted mean age groups: 424±3 Ma (MSWD=0.45) and 402±3 Ma (MSWD=1.4), which were interpreted as granulite-facies metamorphic and retrograde ages, respectively. LA-ICPMS U-Pb dating of zircons from the leucosome sample yields a weighted mean age of 426±2 Ma (MSWD=0.3), which is interpreted as the crystallization age of the leucosome. These data indicate that the West QOB experienced early Paleozoic granulite-facies metamorphism and anatexis similar to the East QOB. However, it remains unclear whether the early Paleozoic granulite facies metamorphism resulted from an arc setting created by the northward subduction of the Shangdan ocean or from a continental collisional orogenic event.

Keywords West Qinling, Granulite, Migmatite, U-Pb age dating, Metamorphism, Early Paleozoic

Citation: Mao X H, Zhang J X, Yu S Y, Li Y S, Yu X X, Lu Z L. 2017. Early Paleozoic granulite-facies metamorphism and anatexis in the northern West Qinling orogen: Monazite and zircon U-Pb geochronological constraints . Science China Earth Sciences, 60: 943–957, doi: 10.1007/s11430-016-9029-7

1. Introduction

Granulite-facies rocks are considered to be a major component of the lower crust within an orogenic belt. These rocks are a window with which to decipher the properties of the lower crust in these regions (Wei et al., 2016). Granulite-facies metamorphism and partial melting often simultaneously occur and have a close relationship with the formation of granite and the differentiation of the Earth's crust (Vanderhaeghe, 2009; Korhonen et al., 2015). Moreover, partial melting strongly influences the thermal and rheological behavior of the lower crust, and plays an important role for the transformation from compression to extension, deep crustal

* Corresponding author (email: zjx66@yeah.net)

flow and exhumation in orogenic belts (Brown et al., 2011 and references therein). Therefore, investigation of the metamorphism and anatexis of the exhumed granulite-facies rocks in an ancient orogenic belt can provide important constraints on the origin of granites, crustal growth and reworking, and orogenic mechanisms. The accurate dating of granulite-facies metamorphism and partial melting is significant toward the better understand of the evolution history of the orogenic belt.

The Qinling orogen experienced multiple stages of oceanic subduction, terrane accretion, and continental collision since the Neoproterozoic (Zhang et al., 1995, 1996, 1997, 2001; Dong et al., 2011b, 2014). It is considered a composite orogenic belt and thus records a cycle of Paleo-Qinling Ocean closure between the North China Block and the South China Block. Traditionally, the Qinling orogen has been subdivided into the South Qingling belt and North Qingling belt by the Shangdan suture, which resulted from the closure of a Paleozoic ocean (Zhang et al., 1995; Meng et al., 1999; Dong et al., 2011b). The Qinling orogen can be further divided into the East Qinling orogen (EQO) and West Qinling orogen (WQO) by the Baoji-Chengdu Railway (Figure 1). As an important part of the North Qinling belt the Qinling Complex (Qinling Group) mainly comprises high-grade metamorphosed supracrustal rocks and intrusive rocks, which collectively represent the deep crustal material of the Qinling orogen (Zhang et al., 2011). Therefore, the Qinling Complex is considered crucial for the understanding of the evolutionary history of the Qinling oeogn as well as reconstruction of the tectonic framework prior to the formation of the Qinling orogen. In the EQO, ultrahigh-pressure (UHP) eclogites (Yang et al., 2002), high-pressure (HP) granulites (Liu et al., 1996, 2009; Zhang et al., 2011) and medium- to low-pressure granulites (Kröner et al., 1993; Zhai et al., 1998; Zhang et al., 2011) have been identified. Abundant geochronological data show that the HP-UHP metamorphic age of the Qinling Complex is between 485 Ma and 507 Ma (Yang et al., 2002; Su et al., 2004; Chen et al., 2004, 2011; Zhang et al., 2011; Liu et al., 2013; Wang et al., 2013), the medium- to low-pressure granulite-facies metamorphic age of the Qinling Complex is between 430 Ma and 450 Ma (Zhang et al., 2009, 2011; Liu et al., 2013; Liu et al., 2011; Xiang et al., 2014), and the amphibolite-facies metamorphic overprinting age is between 420 Ma and 426 Ma (Zhang et al., 2009, 2011; Liu et al., 2013). Extensive anatexis related to granulite-amphibolite facies metamorphism is also recognized (Xiang et al., 2014; Liu et al., 2014). Regional geological data show that the Qinling Complex extends to the west through the Taibai area to the Tianshui region. However, geochronological studies concerning metamorphism of the Qinling Complex usually only focus on the EQO, and as a consequence, geochronological data of the Qingling Complex in the WQO is lacking. Whether the Qinling Complex in the WQO has also experienced multiple stages of early Paleozoic metamorphism is crucial for the determination of the characteristics of Paleozoic orogenies and the reconstruction of orogenic processes. In addition, the WQO is located in a strategic tectonic position linking the Qinling orogen in the east with the Qilian orogenic belt in the west. Studies of the Qinling Complex in the WQO can help to characterize the Paleozoic tectonic framework of the Central Orogen of China.

Recently, based on field geological and petrographic obser-

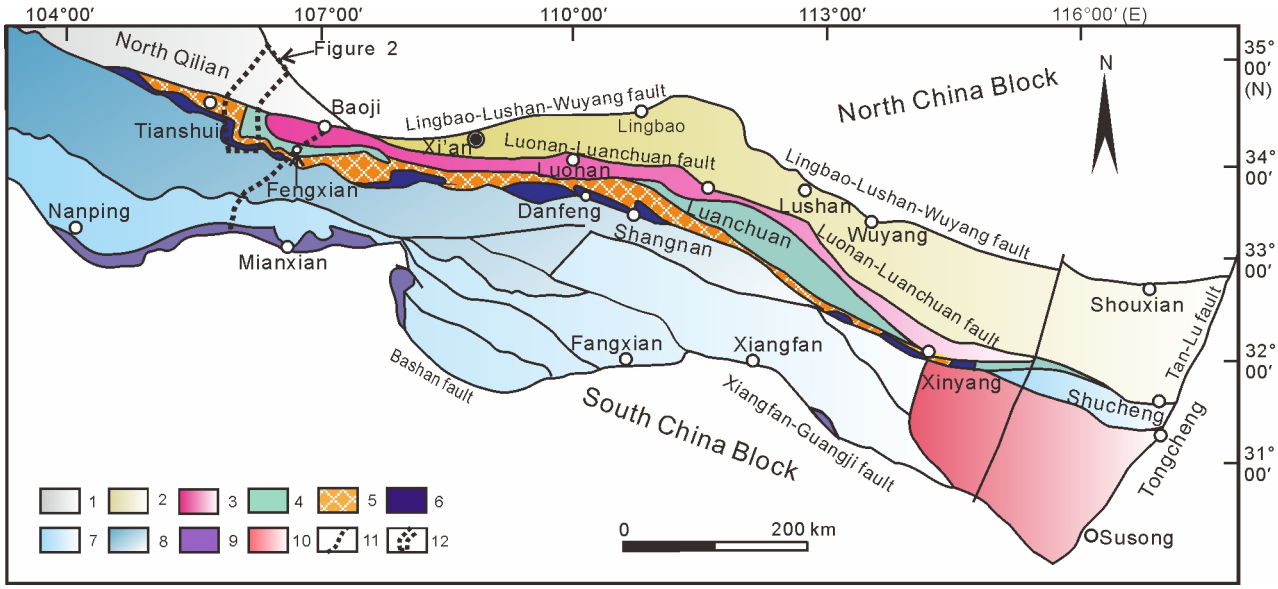

Figure 1 Simplified tectonic map of the Qinling orogen showing the tectonic division and the locality of the studied area (modified after Dong et al., 2011a). 1. North Qilian orogen; 2. Southern margin of the North China Block; 3. Kuanping Group; 4. Erlangping Group; 5. Qinling Complex 6. Shangdan suture; 7. Precambrian Basement-Low Palaeozoic covers; 8. Upper Palaeozoic-Triassic clastic sediments; 9. Mianlue suture; 10. Dabie Terrane; 11. the boundary between the West and East Qinling orogen; 12. study area.

vations, granulite-facies rocks have been recognized within the Qinling Complex in the WQO. In this paper, we present geochronological data using SHRIMP and LA-ICPMS U-Pb dating of zircons and monazites from four representative samples in the Qinling Complex of the WQO in order to constrain the timing of granulite-facies metamorphism and anatexis as well as to provide insight into the early Paleozoic tectonic thermal evolution and the temporal and spatial framework of the Qinling orogen.

2. Geological setting

The Qinling orogen is bounded by the Lingbao-Lushan-Wuyang fault in the north and the Mianlue-Bashan-Xiangguang fault in the south. It has been considered to be a composite orogenic belt that is situated between the North China Block and South China Block (Dong et al., 2011a, 2011b). In the orogen, two ophiolitic sutures are well-documented: the early Paleozoic Shangdan Suture, through which the QOB is divided into the North Qinling belt and the South Qinling belt, and the Mesozoic Mianlue Suture (Dong et al., 2013). Our research area is located in the western region of the North Qinling belt, which is a key tectonic position linking the Qinling orogen with the Qilian orogen (Figure 1). Based on previous data as well as our geological mapping, we divided the western region of the North Qinling belt into three tectonic units (Figure 2): the Liziyuan subduction complex belt (Shangdan Suture), Qinling arc metamorphic-magmatic complex belt and the Qingshui-Zhangjiachuan back-arc complex belt.

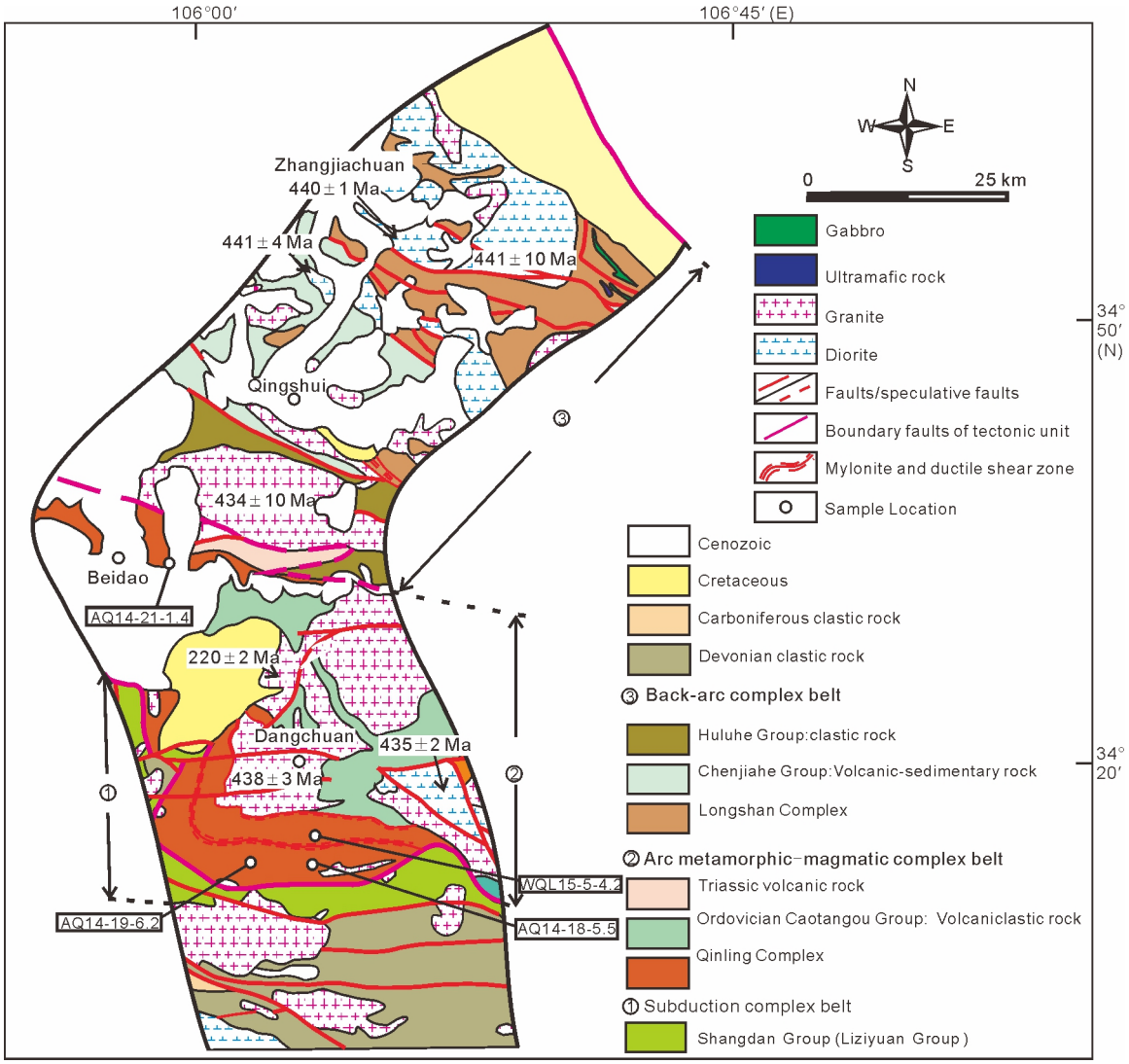

Figure 2 Corridor-like geological map of the northern part of the West Qinling orogen (WQO) showing the tectonic division and sample locations(modified after Xi'an Center of Geological Survey, 2015)[1]. The ages of the plutons are from Pei et al. (2007d, 2012), Zhang et al. (2006a) and Wang et al. (2008).

1) Xi'an Center of Geological Survey. 2015. Geological Map of Qinling Mountain and Neighboring Areas (1:500000).

The Liziyuan subduction complex belt is separated from the Qinling Complex to the north and from the Devonian Dacaotan Group to the south by faults or ductile shear zones. This belt is comprised of low-grade metamorphosed volcanic and sedimentary rocks consisting of greenschist, silty slate, sericite-bearing quartz schist, plagioclase amphibole schist, arkose, andesitic porphyrite and minor lenticular magnetic quartzite. Pei et al. (2004) distinguished a suite of meta-basic volcanic rocks with a typical N-MORB affinity within the Liziyuan Subduction complex belt, which were considered to represent part of an ocean ridge ophiolite and are comparable with the Danfeng Group in the EQO (Pei et al., 2007a).

The Qinling arc metamorphic-magmatic complex belt is separated from the Huluhe Group to the north by the Beidao-Yuanlong ductile shear zone. It is mainly comprised of the high-grade metamorphic Qingling Complex, Caotangou Group volcanic-sedimentary sequence and significant quantities of granitoid and dioritic plutons. The Qinling Complex is separated from the Liziyuan subduction complex belt to the south and the Caotangou Group and Dangchuan granite to the north by ductile shear zones. It consists of orthogneiss and paragneiss units. The orthogneiss units were considered to be derived from Neoproterozoic-age granites with protolith ages between 850−950 Ma (Lu et al., 2005; Pei et al., 2007b). The paragneiss units are composed of garnet-sillimanite gneiss, garnet-biotite schist, marble, calcsilicate rock, quartzite and minor amphibolite (Figure 3). The Caotangou Group mainly consists of volcaniclastic rock and volcanic lava. Based on geochemical data, Yan et al. (2007) suggested that a portion of the volcanic rocks from the Caotangou Group formed within an arc environment related to oceanic subduction. Zircon U-Pb dating yields an Ordovican age (456±2 Ma) for intermediate-basic volcanic rocks from the Caotangou Group (Wang et al., 2007). Silurian and Triassic granitoids and diorites are intruded into the Caotangou Group (Figure 2). The Silurian granites (e.g., the Dangchuan granitoid pluton with a magma crystallization age of 438 Ma) have characteristics of C-type adakite, and are suggested to have resulted from partial melting of the thickened lower crust (Wang et al., 2008; Zhang et al., 2006). Field observations demonstrate that mylonitization and ductile deformation occur along the contact between the Dangchuan granitoid pluton and the Qinling Complex, indicating that the Dangchuan granitoid pluton and the Qinling Complex are separated from each other by a ductile shear zone (Figure 2). However, intermediate and basic igneous complexes (e.g., the Baihua magmatic complex with a magma crystallization age of 435 Ma) show arc-related magma characteristics (Pei et al., 2007c).

The Qingshui-Zhangjiachuan back-arc complex belt is bounded to the south by the Beidao-Yuanlong ductile shear zone and is covered by Quaternary sediments in the north. This belt is composed of the Chenjiahe Group, the Huluhe Group, intermediate-basic igneous plutons and Precambrian basement. The Chenjiahe Group encompasses greenschist-facies meta-basic volcanic rocks, intermediate-acidity volcanic rocks and terrigenous detrital rocks. Basic volcanic rocks that are exposed in the northeastern sector of Tianshui City near the villages of Yangjiasi, Hongtupu and Nantouhe, and represented by the Qingshui section, were labeled as Hongtupu meta-basic rocks in Geological Map of Tianshui with a 1:250000 scale. The Hongtupu meta-basic rocks with a Later Ordovician age are mainly composed of a suite of low-metamorphism greenschist-facies rocks. They are characterized by mid-ocean ridge basalts, and were interpreted to have formed in a back-arc basin setting (He et al., 2007a, 2007b). The acidic volcanic rocks dominantly include meta-rhyolite and dacite with minor dacite, rhyolitic breccia, agglomerate and tuff interlayers. The Huluhe Group, chiefly located near the Qin'an and Qingshui area, is separated from the Hongtupu volcanic rocks to the north by regional ductile faults and from the Qinling Complex to the south by the Xinyang-Yuanlong ductile shear zone. It is mainly composed of a suite of greenschist-facies metamorphosed rocks, and is considered to be derived from terrigenous rocks with a distinct rhythmic structure and Bouma sequence (Wang et al., 2012). The Huluhe Group was previously dated as Neo-

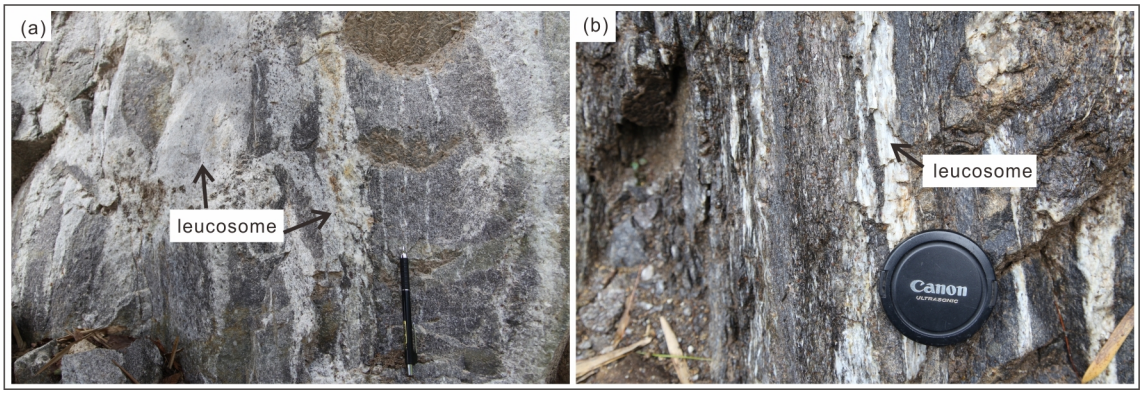

Figure 3 Field pictures of migmatite and migmatitic gneiss of the Qinling Complex in the northern WQO. (a) Migmatite consisting of garnet-bearing leucosome and melanosome; (b) migmatitic garnet-sillimanite gneiss showing strongly ductile deformation.

proterozoic (Xu et al., 2008), but recent dating data of detrital zircons show that it may have formed during the Silurian (Pei et al., 2012). Intrusive rocks primarily consisting of 434−454 Ma granite and diorite were suggested to have developed in an island-arc setting (Zhang et al., 2006; Chen et al., 2007). However, minor mafic intrusive rocks were considered to have formed in a back-arc extensional environment (Chen et al., 2006).

The high-grade gneisses, previously known as the Paleoproterozoic Longshan Group, are exposed within the back-arc complex belt. Both published and unpublished data suggest that the Longshan Group (hereafter designated as "the Longshan Complex") underwent a 1.9 Ga metamorphic event in addition to two magmatic events at 2.35 and 2.5 Ga (He et al., 2005, unpublished data). It is mainly composed of TTG orthogneiss, minor paragneiss and marble. The Longshan Complex is separated from the Paleozoic Chenjiahe Group, Huluhe Group and diorites by faults. Moreover, a great deal of granitoids, diorites, minor gabbro and ultramafic intrusions are also exposed in the back-arc complex belt. They are intruded into or are separated from the other rock units by faults (Figure 2).

3. Field relationship and petrography

The mafic granulite (amphibole-bearing two-pyroxene granulite) WQL15-5-4.2 was sampled near Huamiao Village (34°14.73′N, 106°9.43′E) (Figure 2). This granulite occurs as a lens within the garnet-sillimanite gneiss. The host gneisses show a mylonitic foliation defined by oriented quartz, sillimanite and biotite surrounding garnet porphyroblasts (Figure 4c, d). Sample WQL15-5-4.2 consists of clinopyroxene, orthopyroxene, amphibole, plagioclase, quartz, biotite, ilmenite and minor zircon and apatite (Figure 4a, b). Clinopyroxene, orthopyroxene, plagioclase and quartz show an equilibrium texture. Two stages of amphibole crystallization are recognized: the first consists of brown amphibole that coexists with clinopyroxene, orthopyroxene, and plagioclase, while the second consists of green amphibole that develops around clinopyroxene, orthopyroxene and brown amphibole, and which probably grew during later retrogression. Biotite can also be subdivided into two types. The early-stage brown biotite has a higher TiO_2 content than that of the late-stage biotite growing near the pyroxene rim (see the representative mineral composition in the Appendix

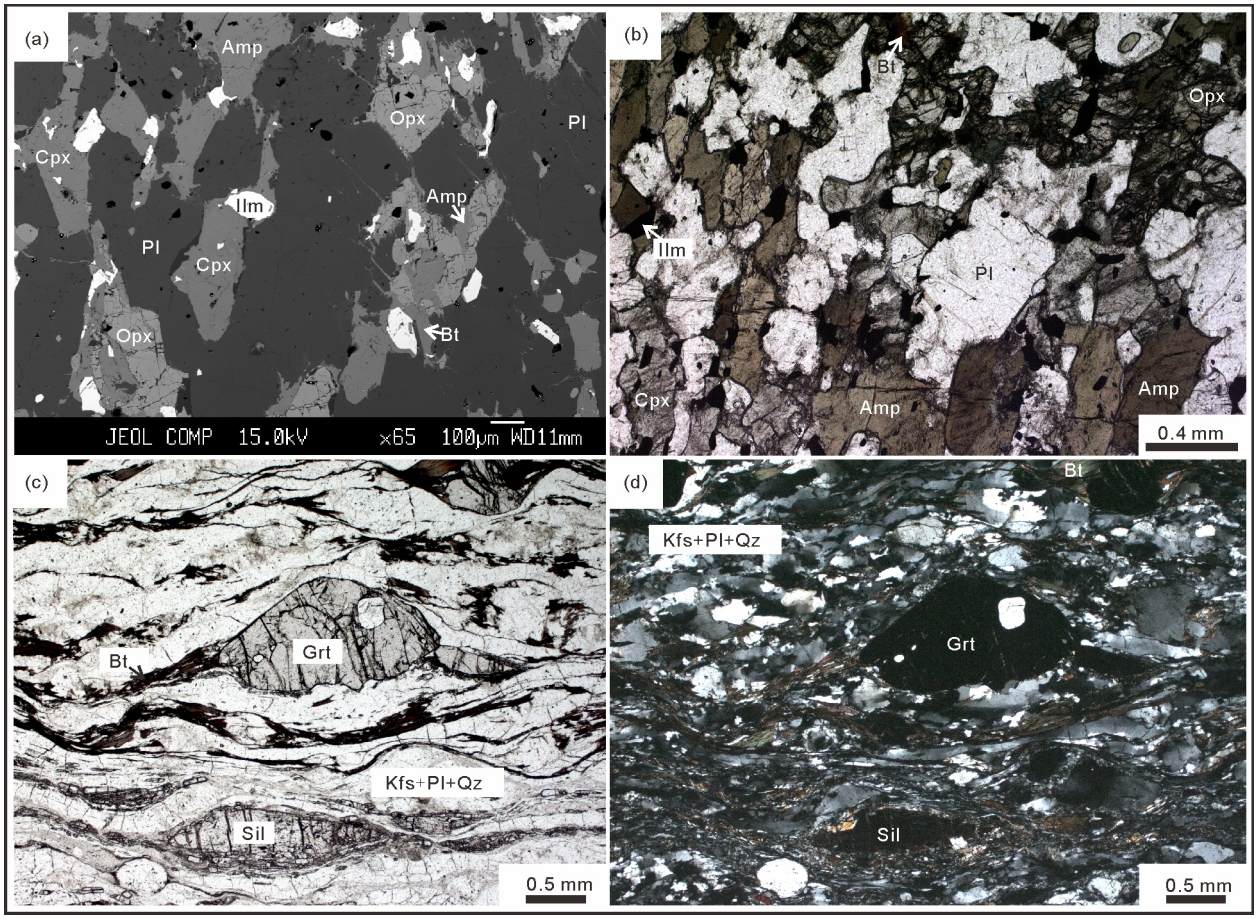

Figure 4 Microtextures of amphibole-bearing two-pyroxene granulite (sample WQL15-5-4.2) and its country rock. (a), (b) Opx-Cpx-Amp-Pl assemblage of amphibole-bearing two-pyroxene granulite ((a) BSE image; (b) phane polarized light); (c), (d) the country rock of amphibole-bearing two-pyroxene granulite consists of garnet, sillimanite, plagioclase, biotite and quartz, and shows strongly ductile deformation ((c) phane polarized light; (d) crossed polarized light).

1 , available at http://earth.scichina.com). Based on textural observations and mineral compositions presented in Appendix 1, the observed peak assemblage is considered to contain clinopyroxene, orthopyroxene, amphibole, plagioclase, quartz, biotite and ilmenite (mineral abbreviations are according to Whitney et al. (2010). The second stage assemblage includes amphibole, plagioclase, quartz, biotite and ilmenite. Based on two-pyroxene geothermometry (Brey et al., 1990), the temperature of the peak assemblage is estimated at 720−800°C. Because of the absence of garnet, the application of geobarometry for pressure estimation is not suitable. The host gneiss with an assemblage of garnet, sillimanite, K-feldspar, plagioclase, biotite and quartz defines a metamorphic condition of 7−7.5 kbar and 779−812°C (unpublished data). However, whether this condition represents the peak condition of granulite remains unclear.

The biotite-bearing garnet-sillimanite gneiss AQ14-18-5.5 unit is sampled (34°12.42′ N, 106°9.83′E) near Huamiao Village. It is mainly composed of garnet, K-feldspar, sillimanite, biotite, plagioclase, and quartz with zircon, monazite and apatite as accessory minerals (Figure 5c), which is similar to the mineral assemblage of the country rock of the mafic granulite. The rock is well-foliated by oriented sillimanite, brown biotite, elongated K-feldspar and recrystallized quartz ribbons, implying that mylonitization is responsible for the development of the observed ribbons. Garnet porphyroblasts are ir-

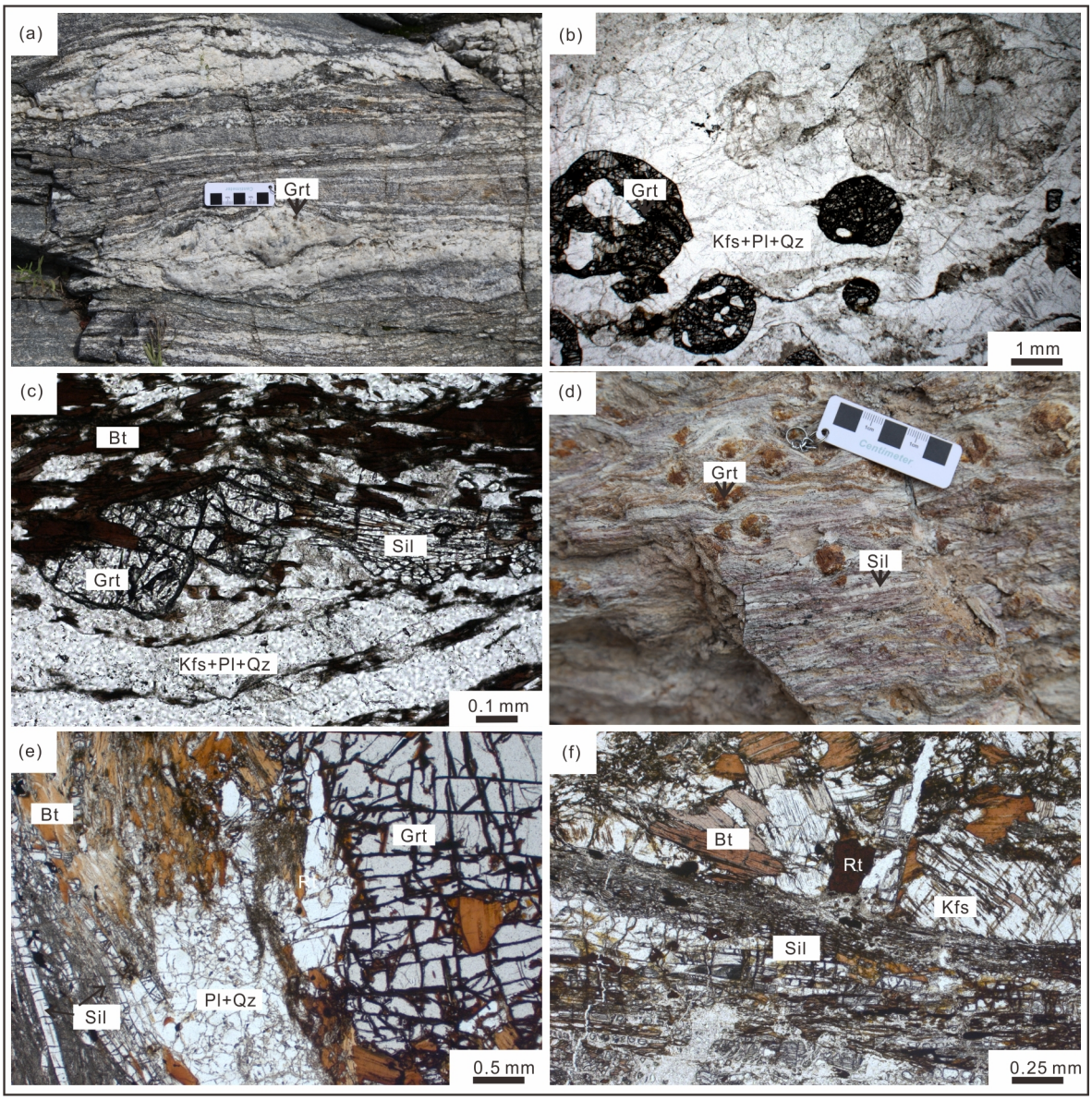

Figure 5 Field pictures and photomicrographs of the representative rocks from the Qinling Complex. (a) The field relationship between leucosome and garnet-sillimanite-biotite gneiss (melanosome) (the scale is 6cm); (b) mineral assemblage of the leucosome AQ14-19-6.2 (phane polarized light); (c) mineral assemblage of garnet-sillimanite-biotite gneiss AQ14-18-5.5 (phane polarized light); (d) field picture of garnet-sillimanite-biotite gneiss AQ14-21-1.4 (phane polarized light, the scale is 6cm long); (e), (f) mineral assemblage of garnet-sillimanite-biotite gneiss AQ14-21-1.4 (phane polarized light).

regular in shape, and possess embayed rims. Sillimanite occurs as needle-like fibers within garnet porphyroblasts or as oriented columnar crystals in the matrix.

The garnet-bearing leucosome AQ14-19-6.2 is sampled near Huamiao Village (34°13.00′N, 106°4.03′E) (Figure 2). It appears as a vein within a biotite-bearing garnet-sillimanite gneiss and parallels the foliation of gneiss (Figure 5a). Its patchy shape implies intensive ductile deformation. The vein is generally 4−23 cm across and consists of K-feldspar, quartz, plagioclase with minor garnet, biotite and white mica. Garnet porphyroblasts occur as 1−5 mm euhedral grains (Figure 5b).

The biotite-bearing garnet-sillimanite gneiss sample AQ14-21-1.4 was collected near Beidao of Tianshui City (34°33.87′N, 105°57.85′E) (Figure 2). In outcrops, this rock has been strongly weathered to a grey brown colour, although 0.5−2 cm garnet grains and oriented sillimanite can be identified (Figure 5d). Sample AQ14-21-1.4 consists of garnet, sillimanite, plagioclase, biotite, K-feldspar, quartz and ilmenite with minor zircon and rutile. Garnet porphyroblasts commonly contain inclusions of biotite, quartz, and rarely spinel and sillimanite. Two distinct morphologies of sillimanite have been recognized. The first occurs as oriented columnar crystals in the matrix, while the second occurs as hair-like crystals along the biotite rim. Biotite also shows two distinct morphologies: one appears as coarse- to medium-grained with red brown flakes defining both the foliation and lineation; the other appears as a fine-grained biotite growing oblique to the dominant foliation in the matrix. Feldspar (plagioclase and K-feldspar) illustrates obvious fracturing, and quartz appears in ribbons (Figure 5e, f).

4. Zircon and monazite age dating

4.1 Analytical methods

The four representative samples mentioned heretofore were selected for zircon and monazite U/Pb analyses. Zircon and monazite grains were separated using conventional heavy liquid and magnetic separation at the Langfang Institute of Regional Geology, Hebei province. Sample mounting, cathodoluminescence (CL) imaging of the zircons and backscattered electron (BSE) imaging were conducted at the Laboratory of Continental Dynamics, Institute of Geology, China Academy of Geological Sciences. Zircon U-Pb dating of sample AQ14-21-1.4 was performed on a SHRIMP-II instrument at the Beijing SHRIMP Center, Institute of Geology, China Academy of Geological Sciences. The monazite U/Pb isotope data of sample AQ14-18-5.5 was collected at the University of California, Santa Barbara (UCSB). Zircon U/Pb dating of samples AQ14-19-6.2 and WQL15-5-4.2 was executed using LA-ICP-MS at the State Key Laboratory of Geological Processes and Mineral Resources, China University of Geosciences (Wuhan).

One hundred of the representative zircon and monazite grains, which have no mineral inclusions or fractures and were sufficiently clean, were first hand-picked under a binocular microscope and were mounted in an epoxy resin thereafter. The sample mount was polished to expose the centers of the zircon grains. Selected zircon grains were photographed in transmitted and reflected light and were imaged using cathode-luminescence. Based on the CL and BSE images, the zircons and monazites suitable for U/Pb analyses was selected for age dating. At the State Key Laboratory of Geological Processes and Mineral Resources, an Agilent 7500a ICP-MS instrument was used to acquire ion-signal intensities, and laser sampling was performed using a GeoLas 2005. Helium was applied as a carrier gas. Argon was used as the make-up gas and was mixed with the carrier gas via a T-connector before entering the ICP. Nitrogen was added into the central gas flow (Ar+He) of the Ar plasma to decrease the detection limit and improve precision (Hu et al., 2008). A “wire” signal smoothing device is included in this laser ablation system, by which smooth signals are produced even at very low laser repetition rates down to 1Hz (Hu et al., 2012). Each analysis incorporated a background acquisition of approximately 20–30 s (a gas blank) followed by 50 s of data acquisition from the sample. The data were evaluated using ICPMSDataCal (Liu et al., 2008). Detailed operating conditions for the laser ablation system and the ICP-MS instrument as well as the data reduction are consistent with the description given by Liu et al. (2010). Zircon unit 91500 was used as the external standard for U-Pb dating, and was analyzed twice for every five analyses. Time-dependent drifts of U-Th-Pb isotopic ratios were corrected using a linear interpolation (with time) for every five analyses according to the variations of 91500 (Liu et al., 2010). Preferred U-Th-Pb isotopic ratios used for 91500 are derived from Wiedenbeck et al. (1995). Concordia diagrams and weighted mean calculations were made using Isoplot/Ex_ver3 (Ludwig, 2003).

Zircon U/Pb dating of sample AQ14-21-1.4 was performed on a SHRIMP-II instrument at the Beijing SHRIMP Center. Detailed analytical procedures were similar to those described by Williams (1998). The intensity of the O^2-ion current was 5 nA , and the ion beam spot size was approximately 25−30 μm in diameter. The procedure utilized standards SL13 and TEM. Age calculations were performed using the Isoplot (Ludwig, 2003) and Squid 11.03d programs, wherein individual analyses were reported with 1σ error and uncertainties in the weighted mean ages were reported at the 95% confidence level.

Monazite U-Pb isotope data of sample AQ14-18-5.5 was collected at the University of California, Santa Barbara (UCSB). The instrumentation consisted of a 193 nm wavelength laser ablation system (Photon Machines, San Diego,

USA) coupled to a Nu Instruments' Nu AttoM SC-ICPM (Nu Instruments, Wrexham, UK). The analytical procedures employed are similar to those described by Cottle et al. (2012, 2013) and Kylander-Clark et al. (2013). Age calculations were performed using Isoplot/Ex_ver3 (Ludwig, 2003). Errors are reported with 2σ standard deviations.

4.2 U-Pb dating results

Zircon grains in sample WQL15-5-4.2 are irregular or round in shape. Zircon grains show fir-tree sector zoning or unzoned structures in CL images, indicating that they were formed during metamorphism (Figure 6). Forty spots were analyzed on 40 zircon grains. All analyses report $^{206}Pb/^{238}U$ ages of 392±5 – 430±6 Ma with Th/U ratios of 0.04−0.26 (most of which are lower than 0.2) (Appendix 2). These data can be further divided into two age clusters in the Concordia diagrams: one cluster yields a weighted mean age of 424±3 Ma (MSWD=0.45), while the other cluster yields a weighted mean age of 402±3 Ma (MSWD=1.4) (Figure 7a).

Monazite grains from sample AQ14-18-5.5 were selected for U/Pb analyses by LA-ICPMS. BSE images demonstrate that most grains are absent a discernable structure or are homogeneous in composition (Figure 6). Thirteen U-Pb spots on 13 monazite grains were analyzed, and the resulting $^{206}Pb/^{238}U$ ages range from 429±13 Ma to 454±14 Ma (Table 1). Of the 13 analyses, 3 analyses report older $^{206}Pb/^{238}U$ ages of 441±14, 447±14 and 454±14 Ma. The remaining 10 analyses yield a weighted mean age of 433±4 Ma (MSWD=0.27) (Figure 7b).

Zircon grains from sample AQ14-19-6.2 present mostly as prismatic and oval crystals. CL images of the zircon grains show a distinct oscillatory zoning (Figure 6). Forty-nine spots were analyzed on 49 zircon grains. The $^{206}Pb/^{238}U$ ages range from 402±6 Ma to 434±8 Ma (Appendix 2) and yield a weighted mean age of 426±2 Ma (MSWD=0.3) (Figure 7c). Most of the analyses (accounting for 88%) contain Th/U ratios lower than 0.12, indicating that they formed during anatexis (Appendix 2).

Zircon grains from sample AQ14-21-1.4 are mostly irregular or round-to-oval in shape. CL images reveal that zircons contain CL-dark or bright CL cores surrounded by unzoned medium-to-dark rims (Figure 6). The zircon cores have two distinct morphologies. One contains distinct oscillatory zoning, and the other shows patchy CL patterns. The zircon rims demonstrate fir-tree sector zoning or unzoned structures in CL images, implying that they formed during metamorphism (Wu et al., 2004). Some of the zircon cores show irregular

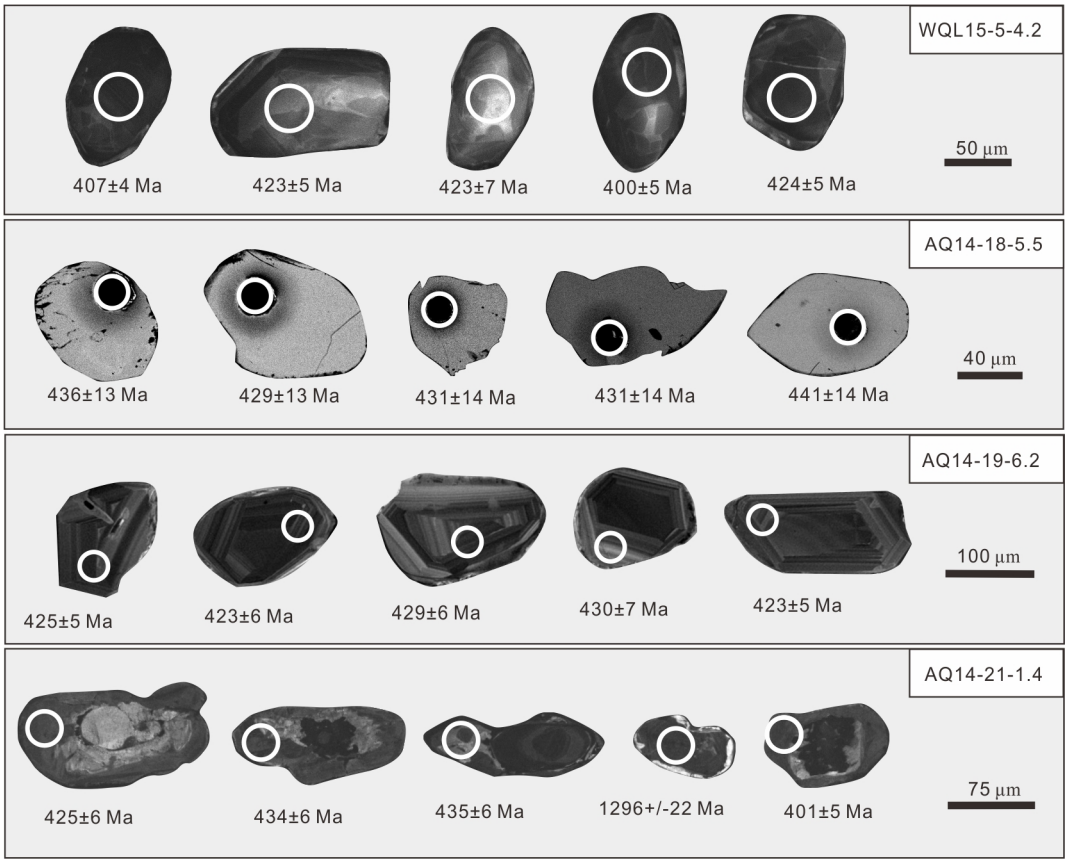

Figure 6 The characteristics of representative CL images of zircons from samples WQL15-5-4.2, AQ14-19-6.2 and AQ14-21-1.4 and BSE images of monazites from sample AQ14-18-5.5.

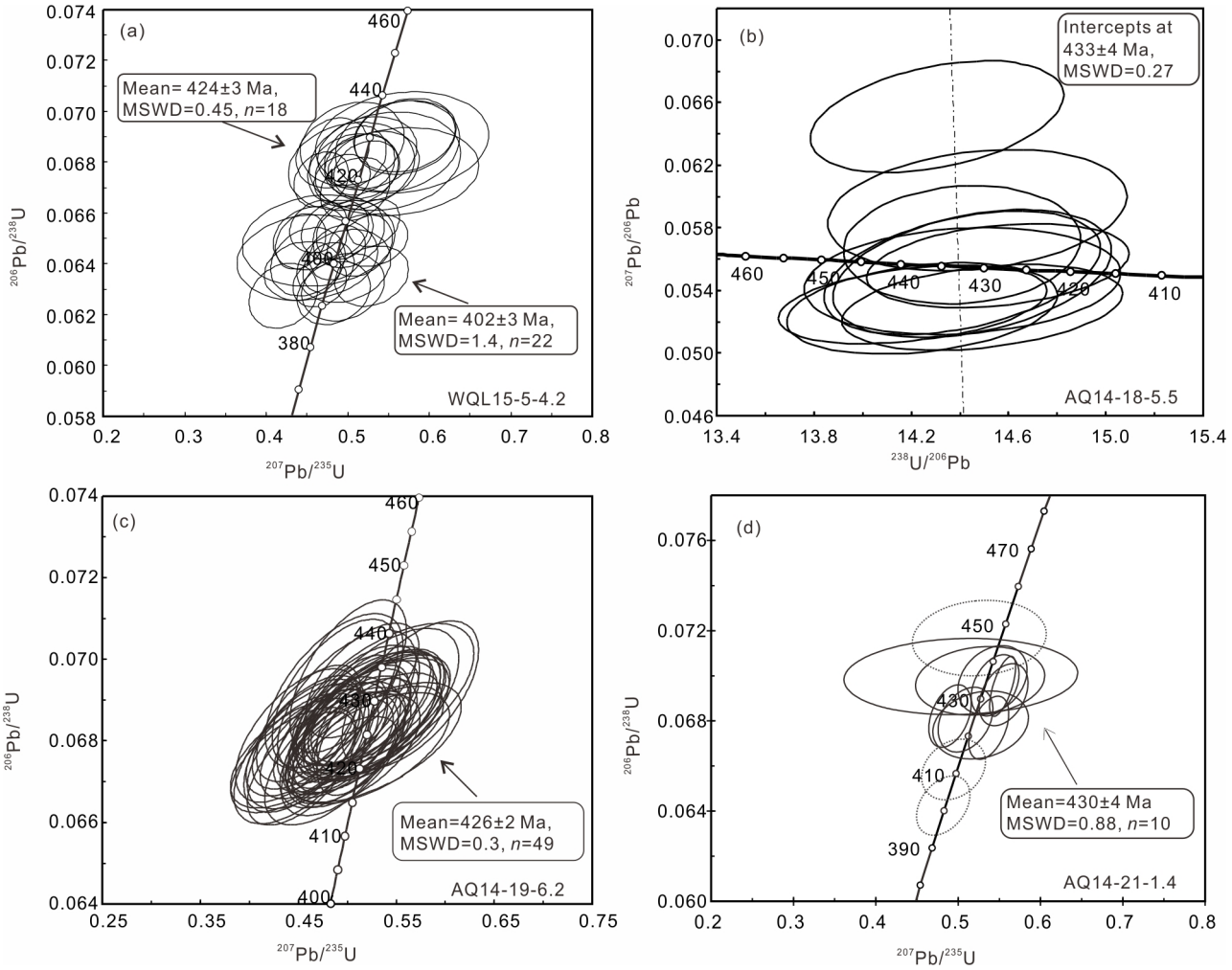

Figure 7 Concordia diagrams for zircon U-Pb analyses and Tera-Wasserburg diagrams for monazite U-Pb analyses. (a), (c), (d) concordia diagrams for zircon U-Pb analyses; (b) Tera-Wasserburg diagrams for monazite U-Pb analyses.

outlines surrounded by a thin semi-continuous luminescent seam, indicating that the core had been resorbed by melt. Twenty spots were analyzed on 20 zircon grains (Table 2). Of the 20 analyses, 13 analyses of the metamorphic domains yield $^{206}Pb/^{238}U$ ages ranging from 401±5 Ma to 446±7 Ma with Th/U ratios between 0.01 and 0.03. With the exception of the two youngest ages (411±6 and 401±5 Ma) and an older age (446±7 Ma), the remaining 11 analyses provide a weighted mean age of 430±4 Ma (MSWD=0.88) (Figure 7d).

5. Discussion

5.1 Silurian granulite-facies metamorphism and anatexis in the West QOB

Over the past fifteen years, a large amount of geochronological data for metamorphic rocks within the Qinling Complex in the East QOB has been reported (Yang et al., 2003; Chen et al., 2004; Zhang et al., 2009, 2011; Li et al., 2012; Liu ea al., 2013; Xiang et al., 2012, 2014a, 2014b; Liu et al., 2011; Wang et al., 2011, 2013a, 2014; Liao et al., 2016; Yu et al., 2016). In contrast, data for metamorphic rocks of the Qinling Complex in the WQO is severely lacking. Based on field investigations as well as petrographic and geochronological data, we suggest that the Qinling Complex in the WQO endured early Paleozoic granulite-facies metamorphism similar to that in the EQO. Mineral assemblages and *P-T* estimation of garnet-sillimanite gneiss AQ14-21-1.4 indicate that this rock underwent a medium-pressure granulite-facies metamorphism, and U-Pb analyses of the metamorphic zircon deliver a weighted mean age of 430±4 Ma (MSWD=0.88). However, linking zircon and monazite growth to metamorphism remains controversial. Some studies have suggested that the growth of zircon is related to the crystallization of melt or retrogression in melt-bearing granulites (Kelsey et al., 2008, 2011; Yakymchuk et al., 2014; Wei, 2016). In contrast, other authors have suggested that the growth of zircon and monazite is related to prograde or peak metamorphic condition in granulites (Hermann et al., 2003; Rubatto et al., 2006; Ewing et al., 2013). In this study, for pelitic granulites in the West

Table 1 LA-ICPMS U-Pb analytical data for monazite from sample AQ14-18-5.5

Spots	Measured ratios							
	$^{207}Pb/^{235}U$	2σ	$^{206}Pb/^{238}U$	2σ	$^{207}Pb/^{206}Pb$	2σ	$^{208}Pb/^{232}Th$	2σ
1	0.5445	0.0317	0.0694	0.0019	0.0548	0.0018	0.0216	0.0004
2	0.5255	0.0301	0.0692	0.0022	0.0549	0.0021	0.0215	0.0004
3	0.6274	0.0269	0.0699	0.0021	0.064	0.0018	0.0223	0.0004
4	0.5265	0.0222	0.0687	0.0021	0.0538	0.0013	0.0219	0.0004
5	0.5155	0.0206	0.0704	0.0022	0.0529	0.0014	0.0219	0.0005
6	0.5275	0.0285	0.0694	0.0022	0.0542	0.0018	0.0223	0.0005
7	0.5634	0.032	0.0691	0.0024	0.0586	0.0019	0.0226	0.0005
8	0.5225	0.0304	0.0694	0.0026	0.0538	0.0017	0.0223	0.0006
9	0.5115	0.024	0.0702	0.0022	0.054	0.0016	0.0229	0.0005
10	0.5035	0.0222	0.069	0.0022	0.0537	0.0014	0.0215	0.0004
11	0.6224	0.0365	0.0708	0.0026	0.0649	0.0024	0.0231	0.0006
Spots	Age (Ma)							
	$^{206}Pb/^{238}U$	2σ	$^{207}Pb/^{235}U$	2σ	$^{207}Pb/^{206}Pb$	2σ	$^{208}Pb/^{232}Th$	2σ
1	433	13	439	21	390	66	432	8
2	431	14	426	19	370	75	431	9
3	436	13	493	18	691	59	446	9
4	429	13	427	16	343	51	439	9
5	438	13	423	14	307	52	438	9
6	434	14	421	18	293	59	446	9
7	431	14	449	21	515	66	453	10
8	434	16	423	19	351	62	448	12
9	437	14	418	16	342	57	459	10
10	431	14	411	14	341	53	432	9
11	441	14	490	22	743	77	463	13

QOB, the metamorphic reaction related to the cooling stage may be represented as: Grt + Ksp + melt = Bt + sill± Pl. This reaction occurs under *P-T* conditions covering a range of 6−9 kbar and a temperature of about 750°C (Spear et al., 1999). Therefore, even though the metamorphic zircon U-Pb age represents the cooling timing of granulite, it still closes to the timing of the peak stage. Moreover, some zircons from garnet-sillimanite gneiss AQ14-21-1.4 contain cores with a hollow or sponge-like structure surrounded by a metamorphic rim. This type of zircon is commonly suggested to form under the presence of fluids (Wu et al., 2004 and references therein). Two analyses of this type of zircon provide ages of 411±6 and 401±5 Ma, indicating that the timing of overprinting amphibolite-facies metamorphism after granulite-facies metamorphism is related to metamorphic fluids.

The CL images and Th/U ratio of zircons from Grt-bearing leucosome AQ14-19-6.2 suggest that they have an anatectic origin. Forty U-Pb analyses from anatectic zircons present a weighted mean age of 426±2 Ma (MSWD=0.3). Large garnet poikiloblasts are commonly recognized in leucosomes of migmatitic pelitic gneisses and are linked to the production of melt (White et al., 2004). Euhedral garnets in leucosome AQ14-19-6.2 and the host paleosome indicate that they are the production of a peritectic reaction (Figure 5a). Therefore, the U-Pb age of zircon from the leucosome, which is consistent with the metamorphic ages of the meta-basic granulite and metapelite within analytical error, represents the crystallization age of the anatectic vein. We thus infer that it closes to the timing of partial melting and granulite-facies metamorphism. Ten U-Pb analyses of monazites from garnet-sillimanite gneiss AQ14-18-5.5 report a weighted mean age of 433±4 Ma (MSWD=0.27), which is consistent with the metamorphic zircon age of garnet-sillimanite gneiss AQ14-21-1.4 within analytical error. In addition, three analyses of monazites from sample AQ14-18-5.5 give a weighted mean age of 447±8 Ma (MSWD=0.82), and one analysis of a zircon from sample AQ14-21-1.4 yields a $^{206}Pb/^{238}U$ age of 446±8 Ma. Considering the dating error, whether these older ages represent an early metamorphism event or different stages of the same event remains unclear. Two age clusters are obtained from mafic granulite WQL15-5-4.2. One age cluster of 424±3 Ma (MSWD=0.45) is consistent with the age of gran-

Table 2 SHRIMP U-Pb analytical data for zircon from sample AQ14-21-1.4[a)]

Spots	$^{206}Pb_c$ (%)	U (ppm)	Th (ppm)	Th/U	$^{206}Pb^*$ (ppm)	$^{207}Pb^*/^{206}Pb^*$	1σ (%)	$^{207}Pb^*/^{235}U$	1σ (%)	$^{206}Pb^*/^{238}U$	1σ (%)	$^{206}Pb/^{238}U$ age (Ma)	$^{207}Pb/^{206}Pb$ age (Ma)
1	1.76	258	4	0.02	15.3	0.0562	7.1	0.5250	7.3	0.0678	1.5	423±6	459±160
2	0.46	509	157	0.32	66.4	0.0794	2.4	1.6550	2.7	0.1512	1.2	908±10	1183±47
3	0.53	285	6	0.02	17.0	0.0580	3.3	0.5530	3.5	0.0692	1.3	431±6	528±72
4	0.05	465	165	0.37	95.0	0.0909	0.61	2.9770	1.4	0.2376	1.2	1374±15	1444±12
5	1.75	276	6	0.02	17.3	0.0528	10	0.5220	11	0.0717	1.5	446±7	321±240
6	1.22	250	32	0.13	21.5	0.0665	6.1	0.9070	6.2	0.0990	1.4	608±8	821±130
7	0.85	225	2	0.01	12.9	0.0542	5.0	0.4920	5.2	0.0658	1.4	411±6	378±110
8	4.45	256	8	0.03	16.1	0.0519	19	0.5010	19	0.0700	1.6	436±7	282±430
9	0.12	250	110	0.46	40.3	0.0841	1.1	2.1720	1.7	0.1872	1.3	1106±13	1296±22
10	3.13	286	32	0.12	23.6	0.0698	10	0.8950	10	0.0931	1.4	574±7	921±210
11	0.08	301	3	0.01	18.0	0.0566	3.3	0.5430	3.5	0.0696	1.3	434±6	475±72
12	1.15	228	2	0.01	13.9	0.0545	9.7	0.5240	9.8	0.0698	1.5	435±6	391±220
13	–	283	388	1.42	47.6	0.0771	0.90	2.0750	1.6	0.1953	1.3	1150±14	1123± 8
14	0.69	316	5	0.02	17.5	0.0542	4.2	0.4800	4.4	0.0642	1.3	401±5	381± 5
15	0.43	236	1	0.01	13.9	0.0519	3.2	0.4880	3.5	0.0682	1.4	425±6	281±74
16	0.20	330	7	0.02	19.2	0.0574	2.7	0.5350	3.0	0.0677	1.4	422±6	506±59
17	0.40	190	1	0.01	11.2	0.0540	4.1	0.5070	4.3	0.0681	1.4	425±6	372±92
18	–	409	10	0.03	24.4	0.0576	1.4	0.5520	1.9	0.0696	1.3	433±5	514±32
19	0.89	220	4	0.02	13.3	0.0560	4.9	0.5390	5.1	0.0698	1.4	435±6	453±110
20	–	64	29	0.48	10.1	0.0843	3.7	2.1650	4.1	0.1862	1.7	1101±17	1300±73

a) Errors are 1σ; Pb_c and Pb^* indicate the common and radiogenic portions, respectively. Common Pb corrected using measured ^{204}Pb.

ulite-facies metamorphism and the crystallization age of the leucosome. Therefore, 424±3 Ma is considered to be the timing of granulite-facies metamorphism. The other age cluster of 402±3 Ma (MSWD=1.4), which is consistent with the two $^{206}Pb/^{238}U$ ages (411±6 and 401±6 Ma) from garnet sillimanite gneiss AQ14-21-1.4 within analytical error, is interpreted as the timing of retrogression (potentially amphibolite facies metamorphism). Generally, based on the heretofore discussion, we suggest that the WQO experienced late Silurian (424−433 Ma or slightly earlier) granulite-facies metamorphism and anatexis followed by a possible amphibolite facies retrogression stage at 402−411 Ma.

5.2 Tectonic implications: are the granulite-facies metamorphism and anatexis related to the Paleozoic magmatic arc or the collisional orogeny?

The aforementioned data suggest that the Qinling Complex of the WQO experienced the Late Ordovician-Silurian medium-low pressure granulite-facies metamorphism similar to that of the Qinling Complex in the EQO, although no Cambrian to Early Ordovicain HP-UHP metamorphism is recognized. There are two opinions concerning the tectonic setting of Late Ordovician-Silurian granulite-facies metamorphism in the EQO: it either formed in a continental arc tectonic setting related to the subduction of the Shangdan Ocean (Xiang et al., 2012, 2014a; Wang et al., 2011, 2013a; Wu et al., 2013), or in a continental collisional setting during the Paleozoic (Kröner et al., 1993; Zhai et al., 1998; Meng et al., 1999; Zhang et al., 2011; Zhang et al., 2013; Liu et al., 2016).

In the northern EQO, recent studies suggest that the arc magmatic rocks have a main age group of 420−450 Ma (e.g., Wang et al., 2013a; Wu et al., 2013). The 420−450 Ma mafic rocks have positive zircon $\varepsilon_{Hf}(t)$ and whole rock $\varepsilon_{Nd}(t)$ values, indicating that they were derived from a relatively depleted mantle. The coeval granitic rocks have variable $\varepsilon_{Hf}(t)$ and $\varepsilon_{Nd}(t)$ values, suggesting crustal growth and reconstruction in the late Ordovician-Silurian. Therefore, some scholars have suggested that high-temperature granulite facies metamorphism, migmatization and arc magmatism simultaneously occurred in the northern EQO, which served as an island arc (or continental arc) in response to the northward subduction of the Paleotethyan Shangdan Ocean during 450−420 Ma (Wu et al., 2013; Xiang et al., 2014b).

In the WQO, the Liziyuan subduction complex belt is located along the southern border of the Qinling Complex. This belt is regarded as an exposure of ophiolitic mélanges near Wushan, Guanzizhen and Tangzang in the Tianshui area (Yang et al., 2006). Metaperidoties, gabbros, plagiogranites and basalts from the Guanzizhen ophiolite illustrate a typical N-MORB affinity with Cambrian-early Ordovician ages (Pei et al., 2004, 2007a) and have been considered to be the west extension of the Shangdan Suture (Pei et al., 2004, 2007b; Yang et al., 2006; Zhang et al., 2004; Zhang et al., 2007, 2006b). Based on geochemical data, the Baihua mafic magmatic complex adjacent to the Qinling Complex was considered to have formed in a magmatic arc setting (Pei et al., 2007c). Zircon U-Pb dating provides an age of 435±2 Ma (MSWD=1.3) for the gabbro of the Baihua mafic magmatic complex, which sheds light on the timing of the northward subduction of the Shangdan ocean and the formation of arc magmatic rocks (Pei et al., 2007c). The 438 Ma Dangchuan granite with C-type adakitic characteristics was suggested to have been generated by the partial melting of the lower crust of the thickening continental margin (Wang et al., 2008). Therefore, similar to the EQO, early Paleozoic granulite-facies metamorphism, anatexis and coeval magmatism also simultaneously occurred in the northern WQO. The granulites and associated migmatites possibly formed in the middle-lower crust of the Paleozoic continental magmatic arc in the northern WQO. This implies that these granulite facies metamorphic rocks are related to the northward subduction of the Shangdan oceanic crust under the Qinling microcontinent. However, these medium-low *P/T* granulite-facies rocks possess characteristics of Barrovian-type metamorphism, which is traditionally considered to be the result of collisional orogenesis. Therefore, the ca. 430 Ma granulite-facies metamorphism can also be recognized as the production of a collisional orogeny. The coeval magmatism can be interpreted as a result of the partial melting of the thickening crust related to continent-continent collisional orogeny. Therefore, in order to clarify the tectonic setting of the late Ordovician-Silurian granulite-facies metamorphism in the Qinling orogen, in addition to further investigation into the metamorphic evolution (*P-T* path) and the tectonic thermal history of the granulites, a comprehensive study combining the regional geology with metamorphic data is required.

6. Conclusions

(1) In the northern WQO, granulite-facies rocks consisting of mafic granulites and pelitic granulites are recognized in the Qinling Complex. These rocks have experienced widespread migmatitization.

(2) Zircon and monazite U-Pb age dating demonstrates that the Qinling Complex of the WQO underwent Late Silurian (424−433 Ma) granulite-facies metamorphism and anatexis, followed by 402−411 Ma amphibolite-facies or retrograde overprinting metamorphism.

(3) It remains unclear whether the early Paleozoic granulite facies metamorphism resulted from an arc setting created by the northward subduction of the Shangdan ocean or from a continental collisional orogenic event.

Acknowledgements *We appreciate the reviewers for their thoughtful*

and constructive reviews on the manuscript. We also thank Cao Hui, Rong He, Li Guangxu and Xie Shiwen for their help with the experimental analyses. This research was supported by the National Natural Science Foundation of China (Grant Nos. 41630207, 41572180) and the China Geological Survey Project (Grant No. 12120115027001).

References

Brey G P, Köhler T. 1990. Geothermometry in four-phase lherzolites. II. New thermobarometers and practical assessment of existing thermobarometers. J Petrol, 31: 1353−1378

Brown M, Schulmann K, White R W. 2011. Granulites, partial melting and the rheology of the lower crust. J Metamorph Geol, 29: 1–6

Chen D L, Liu L, Sun Y, Zhang A D, Liu X M, Luo J H. 2004. LA-ICP-MS zircon U-Pb dating for high-pressure basic granulite from North Qinling and its geological significance. Chin Sci Bull, 49: 2296–2304

Chen D L, Liu L. 2011. New data on the chronology of eclogite and associated rock from Guanpo area, North Qinling orogeny and its constraint on nature of North Qinling HP-UHP eclogite terrane (in Chinese). Earth Sci Front, 18: 158−169

Chen J L, He S P, Wang H L, Xu X Y, Zeng Z X, Wang Z Q, Yan Q R. 2006. Zircon LA-ICPMS U-Pb age of mafic dykes in the area between the Qinling and the Qilian orogenic belts and its geological implications (in Chinese). Acta Petrol Miner, 25: 455−462

Chen J L, Li H B, Wang H L, He S P, Zeng Z X, Xu X Y, Li X M. 2007. LA-ICPMS zircon U-Pb dating diorite pluton from Wangjiacha, the junction area between the Qinling and Qinlian Orogenic Belts and its tectonic significance (In Chinese). J Jilin Univ (Earth Sci Ed), 37: 423−431

Cottle J M, Kylander-Clark A R, Vrijmoed J C. 2012. U–Th/Pb geochronology of detrital zircon and monazite by single shot laser ablation inductively coupled plasma mass spectrometry (SS-LA-ICPMS). Chem Geol, 332-333: 136–147

Cottle J M, Burrows A J, Kylander-Clark A, Freedman P A, Cohen R S. 2013. Enhanced sensitivity in laser ablation multi-collector inductively coupled plasma mass spectrometry. J Anal At Spectrom, 28: 1700–1706

Cumming G L, Richards J R. 1975. Ore lead isotope ratios in a continuously changing earth. Earth Planet Sci Lett, 28: 155–171

Dong Y P, Zhang G W, Neubauer F, Liu X M, Genser J, Hauzenberger C. 2011a. Tectonic evolution of the Qinling orogen, China: Review and synthesis. J Asian Earth Sci, 41: 213–237

Dong Y P, Zhang G W, Hauzenberger C, Neubauer F, Yang Z, Liu X M. 2011b. Palaeozoic tectonics and evolutionary history of the Qinling orogen: Evidence from geochemistry and geochronology of ophiolite and related volcanic rocks. Lithos, 122: 39–56

Dong Y P, Liu X, Neubauer F, Zhang G, Tao N, Zhang Y, Zhang X, Li W. 2013. Timing of Paleozoic amalgamation between the North China and South China Blocks: Evidence from detrital zircon U-Pb ages. Tectonophysics, 586: 173–191

Dong Y P, Yang Z, Liu X M, Zhang X N, He D F, Li W, Zhang F F, Sun S S, Zhang H F, Zhang G W. 2014. Neoproterozoic amalgamation of the Northern Qinling terrain to the North China Craton: Constraints from geochronology and geochemistry of the Kuanping ophiolite. Precambrian Res, 255: 77–95

Ewing T A, Hermann J, Rubatto D. 2013. The robustness of the Zr-in-rutile and Ti-in-zircon thermometers during high-temperature metamorphism (Ivrea-Verbano Zone, northern Italy). Contrib Mineral Petrol, 165: 757–779

He S P, Wang H L, Xu X Y, Zhang H F, Ren G M. 2007a. A LA-ICP-MS U-Pb chronological study of zircons from Hongtubu basic volcanic rocks and its geological significance in the east segment of North Qilian Orogenic Belt (in Chinese). Adv Earth Sci, 22: 143−151

He S P, Wang H L, Xu X Y, Zhang H F, Ren G M. 2007b. Geochemical characteristics and tectonic environment of Hongtubu basalts and Chenjiahe intermediate-acid volcanic rocks in the eastern segment of North Qilian orogenic belt (in Chinese). Acta Petrol Miner, 26: 295−309

He Y H, Sun Y, Chen L, Li H P, Yuan H L, Liu X M. 2005. Zircon U-Pb chronology of Longshan complex by LA-ICPLMS and its geological significance (in Chinese). Acta Petrol Sin, 21: 125−134

Hermann J, Rubatto D. 2003. Relating zircon and monazite domains to garnet growth zones: age and duration of granulite facies metamorphism in the Val Malenco lower crust. J Metamorph Geol, 21: 833–852

Hu Z C, Gao S, Liu Y S, Hu S H, Chen H H, Yuan H L. 2008. Signal enhancement in laser ablation ICP-MS by addition of nitrogen in the central channel gas. J Anal At Spectrom, 23: 1093–1101

Hu Z C, Liu Y S, Gao S, Xiao S Q, Zhao L S, Günther D, Li M, Zhang W, Zong K Q. 2012. A "wire" signal smoothing device for laser ablation inductively coupled plasma mass spectrometry analysis. Spectrochim Acta Part B-Atomic Spectroscopy, 78: 50–57

Kelsey D E, Clark C, Hand M. 2008. Thermobarometric modelling of zircon and monazite growth in melt-bearing systems: Examples using model metapelitic and metapsammitic granulites. J Metamorph Geol, 26: 199–212

Kelsey D E and Powell R. 2011. Progress in linking accessory mineral growth and breakdown to major mineral evolution in metamorphic rock: A thermodynamic approach in the Na_2O-CaO-K_2O-FeO-MgO-Al_2O_3-SiO_2-H_2O-TiO_2-ZrO_2 system. J Metamorph Geol, 29: 151−166

Korhonen F, Brown M, Clark C, Foden J D, Taylor R. 2015. Are granites and granulites consanguineous? Geology, 43: 991−994

Kröner A, Zhang G W, Sun Y. 1993. Granulites in the Tongbai Area, Qinling Belt, China: Geochemistry, petrology, single zircon geochronology, and implications for the tectonic evolution of eastern Asia. Tectonics, 12: 245–255

Kylander-Clark A R C, Hacker B R, Cottle J M. 2013. Laser-ablation split-stream ICP petrochronology. Chem Geol, 345: 99–112

Li Y, Zhou H W, Zhong Z Q,Xiang H, Zeng W, Qi D M, Zhang L. 2012. Two Early-Paleozoic metamorphic events in North Qinling: Petrology and zircon U-Pb geochronology evidences from basic rocks in the Songshugou area (in Chinese). Earth Sci, 37 (Suppl): 111−124

Liao X Y, Liu L, Wang Y W, Cao Y T, Chen D L, Dong Y P. 2016. Multi-stage metamorphic evolution of retrograde eclogite with a granulite-facies overprint in the Zhaigen area of the North Qinling Belt, China. Gondwana Res, 30: 79–96

Liu L, Zhou D W, Wang Y, Chen D L, Liu Yan. 1996. Study and implication of the highpressure felsic granulite in the Qinling complex of East Qinling (in Chinese). Sci China Ser D-Earth Sci, 26 (Suppl): 56−63

Liu L, Chen D L, Wang C, Zhang C L. 2009. New progress on geochronology of high-pressure/ultrahigh-pressure metamorphic rocks from the South Altyn Tagh, the North Qaidam and the North Qinling orogenic, NW China and their geological significance (in Chinese). J Northwest Univ (Nat Sci Ed), 39: 472−479

Liu L, Liao X Y, Zhang C L, Chen D L, Gong X K, Kang L. 2013. Multi-metamorphic timings of HP-UHP rocks in the North Qinling their geological implications (in Chinese). Acta Petrol Sin, 29: 1634−1656

Liu L, Liao X Y, Wang Y W, Wang C, Santosh M, Yang M, Zhang C L, Chen D L. 2016. Early Paleozoic tectonic evolution of the North Qinling Orogenic Belt in Central China: Insights on continental deep subduction and multiphase exhumation. Earth-Sci Rev, 159: 58–81

Liu Q, Wu Y B, Wang H, Gao S, Qin Z W, Liu X C, Yang S H, Gong H J. 2014. Zircon U-Pb ages and Hf isotope compositions of migmatites from the North Qinling terrane and their geological implications. J Metamorph Geol, 32: 177–193

Liu X C, Jahn B M, Hu J, Li S Z, Liu X, Song B. 2011. Metamorphic patterns and SHRIMP zircon ages of medium-to-high grade rocks from the Tongbai orogen, central China: Implications for multiple accretion/collision processes prior to terminal continental collision. J Metamorph Geol, 29: 979–1002

Liu Y S, Hu Z C, Gao S, Günther D, Xu J, Gao C G, Chen H H. 2008. In situ analysis of major and trace elements of anhydrous minerals by

LA-ICP-MS without applying an internal standard. Chem Geol, 257: 34–43
Liu Y S, Gao S, Hu Z C, Gao C G, Zong K Q, Wang D B. 2010. Continental and oceanic crust recycling-induced melt-peridotite interactions in the Trans-North China Orogen: U-Pb dating, Hf isotopes and trace elements in zircons from mantle xenoliths. J Petrol, 51: 537–571
Lu S N, Chen Z H, Li H K, Hao G J, Xiang Z Q. 2005. Two magmatic belts of the Neoproterozoic in the Qinling Orogenic Belt (in Chinese). Acta Geol Sin, 79:165−173
Ludwig K R. 2003. Isoplot 3.00: A geochronological toolkit for microsoft excel. Berkeley Geochronology Center Spec Pub. 1−71
Meng Q R, Zhang G W. 1999. Timing of collision of the North and South China blocks: Controversy and reconciliation. Geology, 27: 123–126
Pei X Z, Ding S P, Hu B, Li Y, Zhang G W, Guo J F. 2004. Definition of the Guanzizhen ophiolite in Tianshui area, western Qinling, and its geological significance (in Chinese). Geol Bull China, 23: 1202−1208
Pei X Z, Ding S P, Li Z C, Liu Z Q, Li G Y, Li R B, Wang F, Li F J. 2007a. LA-ICP-MS zircon U-Pb dating of the gabbro from the Guanzizhen Ophiolite in the northern margin of the Western Qinling and its geological significance (in Chinese). Acta Geol Sin, 81: 1550−1561
Pei X Z, Ding S P, Zhang G W, Liu H B, Li Z C, Li W Y, Liu Z Q, Meng Y. 2007b. Zircons LA-ICP-MS U-Pb dating of Neoproterozoic granitoid gneisses in the north margin of West Qinling and geological implication (in Chinese). Acta Geol Sin, 81: 772−786
Pei X Z, Ding S P, Zhang G W, Liu H B, Li Z C, Li G Y, Liu Z Q, Meng Y. 2007c. The LA-ICP-MS zircons U-Pb ages and geochemistry of the Baihua Basic igneous complexes in Tianshui area of West Qinling. Sci China Ser D-Earth Sci, 50 (Suppl I): 264−267
Pei X Z, Sun Q R, Ding S P, Liu H B, Li Z C, Liu Z Q, Meng Y. 2007d. LA-ICP-MS zircon U-Pb dating of the Yanjiadian diorite in the eastern Qilian Mountains and its geological significance (in Chinese). Geol China, 34: 8−16
Pei X Z, Li Z C, Li R B, Pei L, Liu C J, Gao J M, Wei F H, Wu S K, Wang Y C, Chen Y X. 2012. LA-ICP-MS U-Pb ages of detrital zircons from the meta-detrital rocks of the Early Palaeozoic Huluhe Group in eastern part of Qilian orogenic belt: Constraints of material source and sedimentary age (in Chinese). Earth Sci Front, 19: 205−224
Rubatto D, Hermann J, Buick I S. 2006. Temperature and bulk composition control on the growth of monazite and zircon during low-pressure anatexis (Mount Stafford, Central Australia). J Petrol, 47: 1973–1996
Spear F S, Kohn M J, Cheney J T. 1999. *P-T* paths from anatectic pelites. Contrib Mineral Petrol, 134: 17–32
Su L, Song S G, Sun B, Zhou D W, Hao J Y. 2004. The SHRIMP zircon U-Pb ages of the garnet pyroxenite and Fushui complex from Songshugou area and its constrain on the tectonic evolution of Qinling Oregenic belt (in Chinese). Chin Sci Bull, 49: 1209−1211
Vanderhaeghe O. 2009. Migmatites, granites and orogeny: Flow modes of partially-molten rocks and magmas associated with melt/solid segregation in orogenic belts. Tectonophysics, 477: 119–134
Wang H, Wu Y B, Gao S, Zhang H F, Liu X C, Gong H J, Peng M, Wang J, Yuan H L. 2011. Silurian granulite-facies metamorphism, and coeval magmatism and crustal growth in the Tongbai orogen, central China. Lithos, 125: 249–271
Wang H, Wu Y B, Qin Z W, Zhu L Q, Liu Q, Liu X C, Gao S, Wijbrans J R, Zhou L, Gong H J, Yuan H L. 2013a. Age and geochemistry of Silurian gabbroic rocks in the Tongbai orogen, central China: Implications for the geodynamic evolution of the North Qinling arc-back-arc system. Lithos, 179: 1–15
Wang H, Wu Y B. 2013b. Early Paleozoic HP-UHP metamorphism of the Qinling orogen. Chin Sci Bull, 58: 2124−2131
Wang H, Wu Y B, Gao S, Zhen J P, Liu Q, Liu X C, Qin Z W, Yang S H, Gong H J. 2014. Deep subduction of continental crust in accretionary orogen: Evidence from U-Pb dating on diamond-bearing zircons from the Qinling orogen, central China. Lithos, 190−191: 420−429
Wang H L, Chen L, Sun Y, Liu X M, Xu X Y, Chen J L, Zhang H, Diwu C R. 2007. ~4.1 Ga xenocrystal zircon from Ordovician volcanic rocks in western part of North Qinling Orogenic Belt. Chin Sci Bull, 52: 3002–3010
Wang J, Zhang H F, Xu WC, Cai H M. 2008. Petrogenesis of granites from Dangchuan area in West Qinling Orogenic Belt and its tectonic implication (in Chinese). Earth Sci, 33: 474−486
Wang Y C, Pei X Z, Li Z C, Li R B, Pei L, Wei F H, Liu C J, Gao J M, Wu S K, Chen Y X. 2012. LA-ICP-MS zircon U-Pb dating of the Mesoproterozoic granitic gneisses at Changningyi of Zhangjiachuan area on the eastern edge of the Qilian Orogenic belt (in Chinese). Geol Bull China, 31: 1576−1587
Wei C J, Zhu W P. 2016. Granulite facies metamorphism and petrogenesis of granite (I): Metamorphic phase equilibria for HT-UHT metapelites/greywackes (in Chinese). Acta Petrol Sin, 32: 1611−1624
Wei C J. 2016. Granulite facies metamorphism and petrogenesis of granite (II): Quantitative modeling of the HT-UHT phase equilibria for metapelites and the petrogenesis of S-type granite (in Chinese). Acta Petrol Sin, 32: 1625−1643
White R W, Powell R, Halpin J A. 2004. Spatially-focussed melt formation in alu-minous metapelites from Broken Hill, Australia. J Metamorph Geol, 22: 825−845
Whitney D L, Evans B W. 2010. Abbreviations for names of rock-forming minerals. Am Mineral, 95: 185–187
Williams I S. 1998. U-Th-Pb geochronology by ion microprobe. In: McKibben M A, Shanks W C, Ridley W I, eds. Applications of Microanalytical Techniques to Understanding Mineralizing Processes. Rev Econ Geol, 7: 1−35
Wiedenbeck M, Allé P, Corfu F, Griffin W L, Meier M, Oberli F, Quadt A V, Roddick J C, Spiegel W. 1995. Three natural zircon standards for U-Th-Pb, Lu-Hf, trace element and REE analyses. Geostand Geoanal Res, 19: 1−23
Wu Y B, Zheng Y F. 2004. Genesis of zircon and its constraints on interpretation of U-Pb age. Chin Sci Bull, 49: 1554–1569
Wu Y B, Zheng Y F. 2013. Tectonic evolution of a composite collision orogen: An overview on the Qinling-Tongbai-Hong'an-Dabie-Sulu orogenic belt in central China. Gondwana Res, 23: 1402–1428
Xiang H, Zhang L, Zhong Z Q, Santosh M, Zhou H W, Zhang H F, Zheng J P, Zheng S. 2012. Ultrahigh-temperature metamorphism and anticlockwise *P-T-t* path of Paleozoic granulites from north Qinling-Tongbai orogen, Central China. Gondwana Res, 21: 559–576
Xiang H, Zhong Z Q, Li Y, Qi M, Zhou H W, Zhang L, Zhang Z M, Santosh M. 2014a. Sapphirine-bearing granulites from the Tongbai orogen, China: Petrology, phase equilibria, zircon U-Pb geochronology and implications for Paleozoic ultrahigh temperature metamorphism. Lithos, 208-209: 446–461
Xiang H, Zhong Z Q, Li Y, Zhou H W, Qi M, Lei H C, Lin Y H, Zhang Z M. 2014b. Early Paleozoic polymetamorphism and anatexis in the North Qinling orogeny: Evidence from U-Pb zircon geochronology (in Chinese). Acta Petrol Sin, 30: 2421−2434
Xu X Y, He S P, Wang H L, Zhang E P, Chen J L, Sun J M. 2008. Tectonic framework of North Qinling Mountain and North Qilian Mountain conjunction area in Early Paleozoic: A study of the evidence from strata and tectonic-magmatic events (in Chinese). Northwest Geol, 41: 1−21
Yakymchuk C, Brown M. 2014. Behaviour of zircon and monazite during crustal melting. J Geol Soc, 171: 465–479
Yan Q R, Wang Z Q, Chen J L, Yan Z, Wang T, Li Q G, Jiang C F, Zhang Z Q. 2007. Tectonic setting and SHRIMP age of volcanic rocks in the Xieyuguan and Caotangou Group: Implications for the North Qinling Orogenic Belt (in Chinese). Acta Geol Sin. 81: 488−502
Yang J S, Xu Z Q, Pei X Z, Shi R D, Wu C L, Zhang J X, Li H B, Meng F C, Rong H. 2002. Discovery of Diamond in North Qinling: Evidence for a Giant UHPM Belt across Central China and recognition of Paleozoic and Mesozoic dual deep subduction between North China and Yangtze

Plates. Acta Geol Sin, 76: 484−495
Yang J S, Xu Z Q, Dobrzhinetskaya L F, Green II H W, Pei X Z, Shi R D, Wu C L, Wooden J L, Zhang J X, Wan Y S, Li H B. 2003. Discovery of metamorphic diamonds in central China: an indication of a > 4000-km-long zone of deep subduction resulting from multiple continental collisions. Terra Nova, 15: 370–379
Yang Z, Dong Y P, Liu X M, Zhang J H. 2006. LA-ICP-MS zircon U-Pb dating of gabbro in the Guanzizhen ophiolite, Tianshui, West Qinling, China. Geol Bull China, 25: 1321−1325
Yu H, Zhang H F, Li X H, Zhang J, Santosh M, Yang Y H, Zhou D W. 2016. Tectonic evolution of the North Qinling Orogen from subduction to collision and exhumation: Evidence from zircons in metamorphic rocks of the Qinling Group. Gondwana Res, 30: 65–78
Zhai X M, Day H W, Hacker B R, You Z D. 1998. Paleozoic metamorphism in the Qinling orogen, Tongbai Mountains, central China. Geology, 26: 371–374
Zhang C L, Liu L, Wang T, Wang X X, Li L, Gong Q F, Li X F. 2013. Granitic magmatism related to early Paleozoic continental collision in the North Qinling belt. Chin Sci bull, 58: 4405−4410
Zhang G W, Zhang Z Q, Dong Y P. 1995. Nature of main tectonolithostratigraphic units of the Qinling orogen: Implications for the tectonic evolution (in Chinese). Acta Petrol Sin, 11: 101−114
Zhang G W, Meng Q R, Yu Z P, Sun Y, Zhou D W, Guo A L.1996. Orogenesis and dynamic of the Qinling Qrogen. Sci China Ser D-Earth Sci, 39: 225−234
Zhang G W, Dong Y P, Yao A P. 1997. The crustal compositions, structures and tectonic evolution of the Qinling Orogenic Belt (in Chinese). Geol Shaanxi, 15: 1−14
Zhang G W, Zhang B R, Yuan X C. 2001. Qinling Orogenic Belt and Continent Dynamics (in Chinese). Beijing: Science Press. 1−855
Zhang G W, Guo A L, Yao A P. 2004. Western Qinling-Songpan continental tectonicnode in China's continental tectonics (in Chinese). Earth Sci Front, 11: 23−32
Zhang H F, Jin L L, Zhang Li, Harris N, Zhou L, Hu S H, Zhang B R. 2007. Geochemical and Pb-Sr-Nd isotopic compositions of granitoids from western Qinling belt: Constraints on basement nature and tectonic affinity. Sci China Ser D-Earth Sci, 50: 184−196
Zhang H F, Jin L L, Zhang Li, Yan H L, Zhou L, Zhang B R. 2006b. Pb and Nd Isotopic Compositions of Basement and Granitoid in the Qinlianshan: Constraints on Tectonic Affinity (in Chinese). Earth Sci, 31: 57−65
Zhang J X, Yu S Y, Meng F C, Li J P. 2009. Paired high-pressure granulite and eclogite in collision orogens and their geodynamic implications (in Chinese). Acta Petrol Sin, 25: 2050−2066
Zhang J X, Yu S Y, Meng F C. 2011. Ployphase Early Paleozoic metamorphism in the northern Qinling orogenic belt (in Chinese). Acta Petrol Sin, 27: 1179−1190
Zhang H F, Zhang B R, Harris N, Zhang L, Chen Y L, Chen N S, Zhao Z D. 2006a. U-Pb zircon SHRIMP ages, geochemical and Sr-Nd-Pb isotopic compositions of intrusive rocks from the Longshan-Tianshui area in the southeast corner of the Qilian orogenic belt, China: Constraints on petrogenesis and tectonic affinity. J Asian Earth Sci, 27: 751–764